Fast Advection of Magnetic Fields by Hot Electrons

L. Willingale,[1,2] A. G. R. Thomas,[1,2] P. M. Nilson,[1,*] M. C. Kaluza,[1,†] S. Bandyopadhyay,[3] A. E. Dangor,[1] R. G. Evans,[1] P. Fernandes,[1] M. G. Haines,[1] C. Kamperidis,[1,‡] R. J. Kingham,[1] S. Minardi,[4] M. Notley,[3] C. P. Ridgers,[1] W. Rozmus,[5] M. Sherlock,[1] M. Tatarakis,[4] M. S. Wei,[1,§] Z. Najmudin,[1] and K. Krushelnick[1,2]

[1]*Blackett Laboratory, Imperial College London, London, SW7 2BZ, United Kingdom*
[2]*Center for Ultrafast Optical Science, Nuclear Engineering and Radiological Sciences, University of Michigan, Ann Arbor, Michigan 48109-2099 USA*
[3]*Central Laser Facility, Rutherford Appleton Laboratory, Chilton, Oxon, OX11 0QX, United Kingdom*
[4]*Centre for Plasma Physics & Lasers, Department of Electronics, Technological Educational Institute of Crete, Chania, Crete, Greece*
[5]*Department of Physics, University of Alberta, Edmonton, Alberta, Canada*

(Received 8 December 2009; published 24 August 2010)

Experiments where a laser-generated proton beam is used to probe the megagauss strength self-generated magnetic fields from a nanosecond laser interaction with an aluminum target are presented. At intensities of 10^{15} W cm^{-2} and under conditions of significant fast electron production and strong heat fluxes, the electron mean-free-path is long compared with the temperature gradient scale length and hence nonlocal transport is important for the dynamics of the magnetic field in the plasma. The hot electron flux transports self-generated magnetic fields away from the focal region through the Nernst effect [A. Nishiguchi *et al.*, Phys. Rev. Lett. **53**, 262 (1984)] at significantly higher velocities than the fluid velocity. Two-dimensional implicit Vlasov-Fokker-Planck modeling shows that the Nernst effect allows advection and self-generation transports magnetic fields at significantly faster than the ion fluid velocity, $v_N/c_s \approx 10$.

DOI: 10.1103/PhysRevLett.105.095001 PACS numbers: 52.25.Fi, 52.38.Fz, 52.65.Ff

Extremely large magnetic fields (up to hundreds of megagauss) can be generated through various mechanisms in laser plasma interactions [1–5]. In particular, the $\nabla n_e \times \nabla T_e$ mechanism [1] gives rise to an azimuthal self-generated magnetic field around the laser focal spot when there are nonparallel temperature and density gradients. Braginskii's classical transport theory [6] is commonly employed to describe long-pulse laser interactions, such as inertial confinement fusion (ICF) [7]. In experiments currently being carried out on the National Ignition Facility (NIF), electron temperatures are expected to be such that the electron mean-free-path is long compared with typical gradient scale lengths, and hence nonlocal transport will occur where Braginskii's theory breaks down and kinetic effects become important. Magnetic fields are known to influence the heat flow by inhibiting and localizing transport, but the magnetic field may be advected with the heat flux [8,9]. This coupling of the nonlocal heat fluxes and magnetic field dynamics is poorly understood and yet may be crucial for fully understanding experiments.

Measurements of spontaneously generated magnetic fields have been made using electrical probes [1], Faraday rotation of an external optical beam [2,10,11], or using the polarization properties of the self-generated harmonics [3]. Another probing method, known as proton deflectometry, measures the deflection of a proton beam after it passes through quasistatic electromagnetic fields [12]. Laser generated proton beams produced via the target normal sheath acceleration mechanism have a small virtual source size and excellent laminarity giving good spatial resolution in addition to being well collimated and having a temporal resolution of the order of 1 ps. Proton deflectometry has successfully investigated various phenomena occurring during laser plasma interactions including self-generated magnetic fields around laser focal spots [13–15].

The results presented here investigate magnetic field generation, time evolution, and the resulting plasma dynamics using a proton probing diagnostic. Magnetic fields are detected surprisingly far from the focal spot generation region very early ($\sim$50 ps) in the interaction and subsequently are not observed to change significantly during the remainder of the 1 ns heating pulse. Two-dimensional Vlasov-Fokker-Planck simulations show that under these nonlocal conditions, the magnetic field is rapidly transported away from the generation region into the low density plasma before the magnetic field stagnates because the magnetization has increased. Nonlocal effects in heat flow are important in ICF scenarios because smoothing of nonuniform laser illumination and the subsequent imprinting are relevant to the seeding of the Rayleigh-Taylor instability.

The experiment was carried out using the Vulcan Target Area West facility at the Rutherford Appleton Laboratory. Important requirements for this experiment were the ability to simultaneously measure the plasma density, the magnetic field, the electron temperature (using Thomson scattering), and to image the x-ray emission. The main interaction beam had a pulse duration of 1 ns (rise time of 100 ps), with up to 200 $\pm$ 30 J of energy (assume 50%

in focal spot) at the fundamental wavelength of 1.053 μm. This was focused by an $f/10$ lens (focal length of 1 m) to a spot with a full-width-half-maximum (FWHM) radius of 50 ± 10 μm, giving a laser intensity of $(1.3 \pm 0.8) \times 10^{15}$ W cm^{-2}. The angle of incidence was 45° to the target normal and p polarized. The main interaction targets used were 3 mm $\times$ 5 mm aluminum foils with thicknesses of 25 μm.

The proton beam was generated using a high intensity laser interaction with a solid target [16]. The CPA beam had a pulse duration of 1.5 ps with an energy on target of up to 100 J and was focused with a $f/3.5$ off-axis parabola to a focal spot with a FWHM diameter of 10 μm containing around 40% of the total energy, to achieve peak intensities of 5×10^{19} W cm^{-2}. This pulse interacted with a 20 μm gold foil 2 mm from the main interaction foil to generate the proton beam, which then passed through a 25 μm $\times$ 25 μm mesh before the interaction. The embedding of the mesh structure onto the proton beam enables quantitative measurements of the deflection and hence the electromagnetic field strengths to be made [17]. The magnifications of the mesh and interaction are $M_{\text{mesh}} \approx 20$ and $M_{\text{int}} \approx 10$.

The protons were projected through the rear of the main target and detected on a radiochromic film stack. The signal on a particular layer in the stack will be dominated by a single proton energy population close to their maximum range because of the proton Bragg peak. The electric field of the main interaction, which is dominantly in the target normal direction, should not deflect the protons in this rear projection geometry and are expected to be of sufficiently low amplitude that they do not affect the energy of the proton beam significantly [15]. The deflection due to a magnetic field B extending over a thickness L is given by $d \approx q\text{BL}(b - \frac{L}{2})(2m_pE_p)^{-1/2}$, where d is the deflection in the detector plane and b is the target to detector distance. Both B and L are unknowns. However, the extent of the field, L, may be estimated from the density gradient scale observed by interferometry. If it is assumed that $b \gg L$, then $\mathbf{B} \cdot \mathbf{L} \simeq d(2m_pE_p)^{1/2}/qb$.

A temporally independent transverse optical probe (10 ps, 263 nm) provided information on the electron density and plasma dynamics using a Nomarski interferometer and shadowgraphy [18,19].

The main interaction beam arrives on the target at t_0. Figure 1 shows proton radiographs at times after t_0 of 50, 100, 500, and 800 ps, with the raw images presented in the top row, the images enhanced to show the mesh in the middle row and the magnetic field maps calculated from these images shown in the bottom row. Also shown is a null shot where there was no interaction beam. The heated plasma regions produces a roselike pattern in the proton images and because it is likely that the laser beam contains hot spots, filaments in the plasma are to be expected. A collisional-Weibel instability [20] or an electrothermal instability [21] could be responsible for the density or

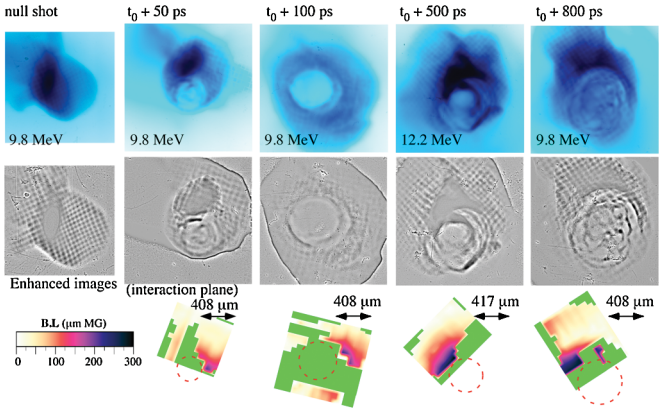

FIG. 1 (color). Proton radiographs using the proton energy indicated on the images to look at a null shot and times after t_0 of 50, 100, 500, and 800 ps. Top panels: raw images. Middle panels: enhanced images. Bottom panels: magnetic field maps. The mesh is too disrupted for measurement in the green regions.

temperature filaments, and perturbations in the heat front should seed such instabilities.

Taking profiles along a number of angles from the center of the focal spot of the magnetic field maps gives average $\mathbf{B} \cdot \mathbf{L}$ products, as a function of distance from the center of the focal spot [Fig. 2]. Although the mesh structure is often unidentifiable in the central regions, at radial distances greater than 150 μm the mesh is visible. After an initially rapid expansion in the first 50 ps of the interaction, the magnetic field does not show significant evolution at later times. The magnetic field strength can be estimated if the extent of the field is approximately the interferometry density scale length, $L \approx 100$–200 μm, giving $B \approx 1$–2 MG. For comparison, the product of transverse electric field strength, E, and thickness, L, required are shown on the top axis of this plot. Estimating

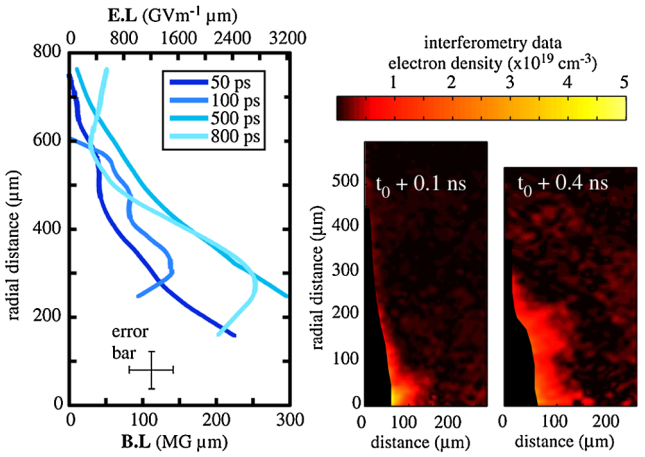

FIG. 2 (color online). Left panel: A plot of the product of the magnetic field and the spatial extent ($\mathbf{B} \cdot \mathbf{L}$) against distance from the focal spot for times after t_0 of 50, 100, 500, and 800 ps. Right panel: Electron density maps of plasma plumes from interferometry at times of t_0 + 100 ps and t_0 + 400 ps.

$L \sim 100$ μm and $E \approx -\nabla(k_B T_e)/e \approx 800$ eV/50 μm $= 16 \times 10^{-3}$ GV m^{-1} suggests that the electric field makes a negligible contribution.

Figure 2 also shows the electron density maps of plasma plumes from aluminum targets at times of $t_0 + 100$ ps and $t_0 + 400$ ps. The plasma expansion speed perpendicular to the target surface is calculated from the optical probing to be of the order of 10^5 ms^{-1}, which is comparable to the sound speed, $c_s = \sqrt{Z k_B T_e/m_i} = 2 \times 10^5$ ms^{-1} [22], where $T_e \approx 800$ eV is the electron temperature measured by Thomson scattering. However, the observed plasma expansion speed along the target surface estimated from the interferometry is 5×10^5 ms^{-1}. Expansion of the fast electrons is expected to be faster along the target surface than normal to it, due to the reservoir of cold electrons available for the return current [23], which can ionize plasma in a region away from the focus. The magnetic field is observed to move radially, much more rapidly [Fig. 2], at ≈ 400 μm/50 ps $= 8 \times 10^6$ ms^{-1}.

It is expected that the magnetic field generation ($\nabla n_e \times \nabla T_e$) should occur predominantly in the focal region, where the plasma is being generated through ionization and heating. If frozen-in-flow is assumed, the magnetic advection velocity would be the ion fluid velocity, which is too slow to explain the appearance of magnetic fields far from the focal region at early times. However, as the hot electrons stream from the focus, they also transport the magnetic fields via the Nernst effect. This is a theoretically well-known effect [8,9], arising from the velocity dependence of the collision frequency, which makes it easier for slower electrons to diffuse across magnetic field lines. It is related to the electron heat flux, which is dominated by the faster particles, those with 2–3 times the electron thermal velocity, v_{T_e}, and has recently been demonstrated in simulations to advect magnetic field at a rate much faster than frozen-in-flow [24]. There are numerous other mechanisms, which could excite magnetic fields; however, such higher order effects should be far less significant.

The electron transport is described under these conditions by the Vlasov-Fokker-Planck equation with relevant heating operators, and with fields and currents being coupled by Faraday's and Ampére's laws. When appropriate moments are taken, the Lorentz term, $\mathbf{v} \times \mathbf{B} \cdot (\frac{\partial f}{\partial \mathbf{v}})$ in the kinetic equation gives rise to a term in a generalized Ohm's law, $\mathbf{v}_N \times \mathbf{B}$. When combined with Faraday's law, this yields an advection equation to describe the evolution of the magnetic field [9]; $\dot{\mathbf{B}} + \nabla \times [(\mathbf{C} + \mathbf{v}_N) \times \mathbf{B}] = 0$, where $\mathbf{C}$, the plasma flow velocity, has been specifically included. Assuming a locally defined Maxwellian electron distribution function, the classical transport equations of Braginskii [6] can be used to express the Nernst velocity, with a collision frequency which scales as v^{-2} [9], as $\mathbf{v_N} \approx 2\mathbf{q_e}/5 n_e T_e$, where $\mathbf{q_e} = -n_e T_e \tau_{ei} \underline{\kappa}^c \cdot \nabla T_e/m_e$, is the classical Braginskii heat flux (ignoring the current contribution), with $\underline{\kappa}^c$ being the normalized thermal conductivity tensor [25]. An *estimate* of the lateral Nernst velocity is $\mathbf{v_N} = 1.3 \times 10^6 \kappa_\perp$ ms^{-1}, based on the experimental parameters using a characteristic temperature gradient scale length of the focal spot size and assuming full ionization. The thermal conductivity in the radial direction, $\kappa_\perp^c$, depends on the local Hall parameter, $\omega_c \tau_{ei}$, which is estimated to be less than 1 at the critical surface, where $\omega_c = eB/m_e$ and τ_{ei} is the electron ion collision time. $\kappa_\perp^c$ has a value of 13.6 for low magnetization ($\omega_c \tau_{ei} \ll 1$), and falls off to $\kappa_\perp^c \approx 1$ for $\omega_c \tau_{ei} = 1$ [25].

Two-dimensional modeling of the experiment was performed using IMPACTA, an implicit, finite-difference, Vlasov-Fokker-Planck code, which uses a Cartesian tensor expansion of the distribution function [26,27]. In this model, the kinetic equations are solved for the electron distribution, but ions are treated as a cold (but mobile) fluid which is initially stationary. Figure 3 illustrates the geometry of the simulation plane and the initial density profile based on a fully ionized aluminum plasma approximating the early time interferometric data. The plasma was heated from an initial temperature of 20 eV using Langdon's inverse bremsstrahlung operator [28] for a laser intensity of 10^{15} W cm^{-2}.

Strong magnetic fields are generated in the high density region near the focal spot through $\nabla n_e \times \nabla T_e$ and other mechanisms and are rapidly advected into the low density region and across the target surface. By examining the contributions to the electric field, the simulation indicates that the hot electrons both advect the field through the Nernst effect and also spontaneously generate fields through a nonlocal version of the $\nabla n_e \times \nabla T_e$ mechanism [4]. Ionization effects, which are not currently included in the code, may also play a role. The Nernst velocity in the simulations is calculated directly via $\mathbf{v_N} = \langle \mathbf{v} v^3 \rangle / \langle v^3 \rangle$—where the angle brackets indicate the expectation of the quantity within the brackets—through integration with the electron distribution function calculated by the code. The factor v^3 arises because of the velocity dependence of the electron-ion collisions, which is factored out in formulating Ohm's law. By 50 ps the magnetic field stagnates at a distance of up to 400 μm from the interaction region.

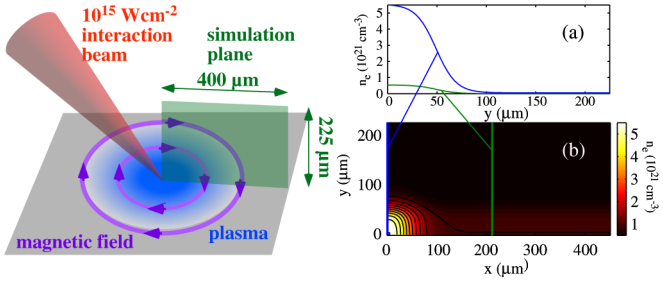

FIG. 3 (color online). The 2D simulation plane is perpendicular to the target surface, with the heating occurring at one end of the box so that the magnetic field expansion can be observed. (a) and (b) are the initial n_e profiles.

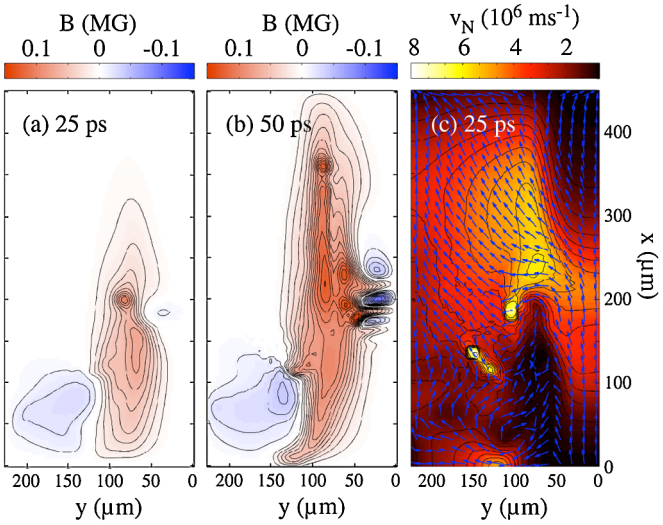

FIG. 4 (color online). The simulation results showing (a) and (b) the magnetic field profile at 25 and 50 ps, respectively. (c) Nernst velocity, $\mathbf{v_N}$, at 25 ps, calculated directly from the distribution function.

The ion velocity is predominantly perpendicular to the target surface and is orders of magnitude too slow to account for the magnetic field advection.

In Figs. 4(a) and 4(b), magnetic field profiles are shown at 25 and 50 ps, respectively, demonstrating an average advection velocity of the fields of around 400 μm/50 ps $= 8 \times 10^6$ ms^{-1}, in good agreement with the experiment. Figure 4(c) shows $\mathbf{v_N}$ calculated directly from the electron distribution at 25 ps. At later times, $\mathbf{v_N}$ is still high, but forms eddies rather than a linear flow, forming stagnated regions of high magnetization sufficient to form a magnetic transport barrier.

In conclusion, proton deflectometry has been used to measure self-generated magnetic fields from $I \sim 10^{15}$ W cm^{-2} nanosecond laser interactions with aluminum targets. The rapid radial expansion of the measured magnetic fields is not consistent with magnetohydrodynamic theory but is predicted by 2D kinetic modeling where it appears as a combination of the Nernst effect and nonlocal magnetic field generation. The magnetic fields are intrinsically coupled to the hot electron dynamics, can be rapidly transported and can also form transport barriers. Measurements of this phenomenon are of fundamental interest in understanding magnetic fields in laser-heating scenarios, and in particular, for ICF experiments currently being conducted at NIF, where although the gradient scale lengths are larger, the high electron temperature results in a very long electron mean-free-path.

The authors acknowledge the staff of the Central Laser Facility at the Rutherford Appleton Laboratory for technical assistance. This work was supported by the UK EPSRC. IMPACTA was developed under EPSRC Grant No. EP/C531566/1. The simulations were performed on the Nyx cluster at the University of Michigan. M. T. was supported by the E.U. through the Marie Curie Transfer of Knowledge grant DAIX Contract No. MTKD-CT- 2004-014423.

*Present address: LLE and FSC, University of Rochester, Rochester NY, USA.
†Present address: Institute for Optics and Quantum Electronics, Jena, Germany.
‡Present address: Technological Educational Institute of Crete, Chania, Crete, Greece.
§Present address: Center for Energy Research, University of California, San Diego, California, USA.

[1] J. A. Stamper *et al.*, Phys. Rev. Lett. **26**, 1012 (1971).
[2] M. Borghesi *et al.*, Phys. Rev. Lett. **80**, 5137 (1998).
[3] M. Tatarakis *et al.*, Nature (London) **415**, 280 (2002).
[4] R. J. Kingham and A. R. Bell, Phys. Rev. Lett. **88**, 045004 (2002).
[5] U. Wagner *et al.*, Phys. Rev. E **70**, 026401 (2004).
[6] S. I. Braginskii, *Transport Properties in a Plasma*, Review of Plasma Physics Vol. 1, edited by M. A. Leontovish (Consultants Bureau, New York, 1966), p. 205.
[7] J. Lindl, Phys. Plasmas **2**, 3933 (1995).
[8] A. Nishiguchi *et al.*, Phys. Rev. Lett. **53**, 262 (1984).
[9] T. H. Kho and M. G. Haines, Phys. Rev. Lett. **55**, 825 (1985)
[10] J. A. Stamper, E. A. McLean, and B. H. Ripin, Phys. Rev. Lett. **40**, 1177 (1978).
[11] A. Raven, O. Willi, and P. T. Rumsby, Phys. Rev. Lett. **41**, 554 (1978).
[12] M. Borghesi *et al.*, Laser Part. Beams **20**, 269 (2002).
[13] C. K. Li *et al.*, Phys. Rev. Lett. **97**, 135003 (2006).
[14] S. Le Pape *et al.*, Astrophys. Space Sci. **307**, 341 (2007).
[15] C. A. Cecchetti *et al.*, Phys. Plasmas **16**, 043102 (2009).
[16] E. L. Clark *et al.*, Phys. Rev. Lett. **84**, 670 (2000); A. Maksimchuk *et al.*, *ibid.* **84**, 4108 (2000); R. A. Snavely *et al.*, *ibid.* **85**, 2945 (2000).
[17] A. J. Mackinnon *et al.*, Rev. Sci. Instrum. **75**, 3531 (2004).
[18] P. M. Nilson *et al.*, Phys. Rev. Lett. **97**, 255001 (2006).
[19] P. M. Nilson *et al.*, Phys. Plasmas **15**, 092701 (2008).
[20] E. M. Epperlein, Plasma Phys. Controlled Fusion **27**, 1027 (1985).
[21] M. G. Haines, Phys. Rev. Lett. **47**, 917 (1981).
[22] R. S. Marjoribanks *et al.*, Phys. Rev. Lett. **45**, 1798 (1980).
[23] R. Decoste, J.-C. Kieffer, and H. Pépin, Phys. Rev. Lett. **47**, 35 (1981).
[24] C. P. Ridgers, R. J. Kingham, and A. G. R. Thomas, Phys. Rev. Lett. **100**, 075003 (2008).
[25] E. M. Epperlein and M. G. Haines, Phys. Fluids **29**, 1029 (1986).
[26] A. G. R. Thomas, R. J. Kingham, and C. P. Ridgers, New J. Phys. **11**, 033001 (2009).
[27] R. J. Kingham and A. R. Bell, J. Comput. Phys. **194**, 1 (2004).
[28] A. B. Langdon, Phys. Rev. Lett. **44**, 575 (1980).